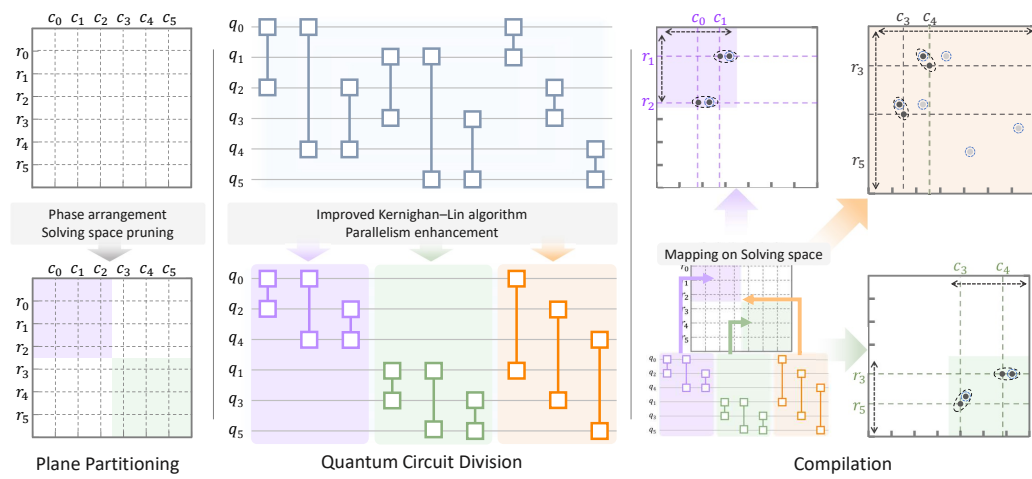


Graphical Abstract

Physics-Aware Compilation for Parallel Quantum Circuit Execution on Neutral Atom Arrays

Geng Chen, Guowu Yang, Wenjie Sun, Lianhui Yu, Guangwei Deng, Desheng Zheng, XiaoYu Li[†]



Highlights

Physics-Aware Compilation for Parallel Quantum Circuit Execution on Neutral Atom Arrays

Geng Chen, Guowu Yang, Wenjie Sun, Lianhui Yu, Guangwei Deng, Desheng Zheng, XiaoYu Li[†]

- Presents **Physics-Aware Compilation** balancing efficiency with flexibility in neutral atom quantum systems.
- Achieves parallel quantum circuit execution through hardware plane partitioning and improved Kernighan-Lin algorithm.
- Delivers up to $202.81\times$ speedup while maintaining comparable circuit quality across various array sizes.

Physics-Aware Compilation for Parallel Quantum Circuit Execution on Neutral Atom Arrays

Geng Chen^a, Guowu Yang^a, Wenjie Sun^b, Lianhui Yu^c, Guangwei Deng^d,
Desheng Zheng^{f,1}, XiaoYu Li^{†g}

^a*School of Computer Science and Engineering, University of Electronic Science and Technology of China, Cheng Du, 610054, Si Chuan, China*

^b*School of Electronic Science and Engineering, University of Electronic Science and Technology of China, Cheng Du, 610054, Si Chuan, China*

^c*School of Physics, University of Electronic Science and Technology of China, Cheng Du, 610054, Si Chuan, China*

^d*Institute of Fundamental and Frontier Sciences, University of Electronic Science and Technology of China, Cheng Du, 610054, Si Chuan, China*

^e*Kash Institute of Electronics and Information Industry, Kashgar, 844199, XinJiang, China*

^f*School of Computer Science and Software Engineering, Southwest Petroleum University, Cheng Du, 610599, Si Chuan, China*

^g*School of Information and Software Engineering, University of Electronic Science and Technology of China, Cheng Du, 610054, Si Chuan, China*

Abstract

Neutral atom quantum computers are one of the most promising quantum architectures, offering advantages in scalability, dynamic reconfigurability, and potential for large-scale implementations. These characteristics create unique compilation challenges, especially regarding compilation efficiency while adapting to hardware flexibility. However, existing methods encounter significant performance bottlenecks at scale, hindering practical applications. We propose **Physics-Aware Compilation (PAC)**, a method that improves compilation efficiency while preserving the inherent flexibility of neutral atom systems. PAC introduces physics-aware hardware plane partitioning that strategically allocates hardware resources based on physical device characteristics like AOD and SLM trap properties and qubit mobility constraints. Additionally, it implements parallel quantum circuit division with an improved Kernighan-Lin algorithm that enables simultaneous execution across independent regions while maintaining circuit fidelity. Our experimental evaluation compares PAC with state-of-the-art methods across

increasingly larger array sizes ranging from 16×16 to 64×64 qubits. Results demonstrate that PAC achieves up to $78.5\times$ speedup on 16×16 arrays while maintaining comparable circuit quality. PAC’s compilation efficiency advantage increases with system scale, demonstrating scalability for practical quantum applications on larger arrays. PAC explores a viable path for practical applications of neutral atom quantum computers by effectively addressing the tension between compilation efficiency and hardware flexibility. Code for PAC is available.

Keywords: Neutral Atom Quantum Computing, Quantum Compilation, Qubit Mapping, Physics-Aware Optimization

1. Introduction

Quantum computing has powerful parallel computing capabilities and has the potential to solve optimization problems[1], perform chemical simulations[2], solve linear systems of equations[3], etc. In order to better utilize the advantages of quantum computing, a variety of hardware technology routes have been proposed to achieve real quantum computing, including superconducting[4], quantum dot[5], atom arrays[6], etc. Among these platforms, neutral atom quantum computing has attracted growing interest due to its advantages in large-scale quantum computation and inherent reconfigurability, offering flexibility in qubit arrangement and interaction.

Quantum compilation is an essential process for deploying quantum circuits onto quantum computers. It involves transforming a quantum circuit into an executable sequence of operations that can be implemented on quantum hardware to achieve the intended functionality. The quantum compilation approach varies significantly depending on the underlying quantum hardware architecture. Currently, most quantum compilation research focuses on superconducting quantum computers, encompassing solver-based methods [7, 8, 9], heuristic approaches [10, 11, 12], and other techniques. Recently, neutral atom quantum computers have attracted growing interest due to their advantages in large-scale quantum computation [13] and their inherent reconfigurability [14]. Unlike superconducting quantum computers, the hardware implementation of quantum operations in neutral atom systems is not strictly constrained by swap gates. By trapping atoms that serve as qubit carriers in an optical tweezer array [6], individual qubits can be flexibly transported and brought into proximity with one another. This mobility

facilitates the formation of entanglement and enables an extended quantum lifetime [15].

However, this flexibility introduces a critical paradox in quantum compilation: existing methods either optimize compilation efficiency at the expense of hardware flexibility, or preserve flexibility while suffering performance bottlenecks. This tension becomes particularly acute as system sizes increase, with compilation times for neutral atom platforms reaching hours for moderately-sized circuits. Such inefficiency severely constrains the practical utility of neutral atom quantum computers despite their theoretical advantages.

As an attempt to address this key contradiction, a series of fruitful efforts have been put forward. Baker[16]introduced a layered compilation approach for quantum circuits. However, the inter-layer scheduling introduced additional execution time. In 2023, Li et al. [17] proposed a greedy algorithm incorporating Monte Carlo tree search to optimize circuit compilation. Patel et al. presented GRAPHINE [18], which utilizes an annealing-based approach for qubit position arrangement. As a mainstream solution, reconfigurable quantum processors have been developed [6]. These architectures enable flexible atomic repositioning, facilitating entanglement between different qubits and achieving enhanced connectivity, programmability, and parallelism. Leveraging this architecture, Tan et al. (2022) proposed the first solver-based compilation method for neutral atoms [19]. In 2024, Tan et al. introduced DPQA[20], which integrates the advantages of greedy algorithms and solver-based approaches to improve both computational efficiency and scalability. In the same year, Ludmir et al. proposed PARALLAX [21], an extension of the GRAPHINE method that enhances circuit execution fidelity.

While these approaches have shown promise, they fail to effectively address the fundamental tension between leveraging the platform’s inherent parallelization potential and maintaining its flexible reconfigurability. As a result, existing compilation methods for neutral atom quantum computers fail to fully exploit their inherent parallelization potential and the resulting improvements in efficiency. These approaches treat the compilation problem as primarily computational rather than recognizing it as inherently problems in the physical scene—a perspective shift that could potentially resolve the parallelism-flexibility paradox.

As a response to this motivation, we propose a physics-aware compilation (PAC) approach for neutral atom quantum computers. PAC recognizes that the unique physical characteristics of neutral atom hardware can guide com-

pilation decisions. PAC introduces a Physics-Aware Hardware Plane Partitioning method that strategically allocates hardware resources based on the physical characteristics of the device. This hardware-aware approach effectively prunes the solution space at the hardware level while enabling optimal task allocation. Furthermore, PAC implements Parallel Quantum Circuit Division with an improved Kernighan-Lin algorithm that divides qubits of the target circuit into two communities with tight internal connections and fewer cross-community relationships. This approach enables simultaneous execution across independent regions while maintaining circuit fidelity, enhancing compilation parallelism and ultimately improving overall efficiency. Together, these techniques address the critical tension between compilation speed and hardware flexibility. The main contribution of this paper is:

1. This work focuses on the critical tension between compilation efficiency and hardware flexibility in neutral atom quantum computing. By analyzing physical properties of neutral atom systems, a physics-aware compilation approach is proposed that significantly improves efficiency while preserving the platform’s inherent reconfigurability.
2. A two-component framework is developed, consisting of Hardware Plane Partitioning for physics-guided resource allocation and Quantum Circuit Division. This approach effectively transforms complex global compilation challenges into manageable local optimization problems while respecting hardware constraints.
3. Extensive experimental evaluation across multiple array scales demonstrates PAC’s performance on diverse benchmark circuits. PAC achieves up to $78.5\times$ speedup compared to SOTA method. PAC successfully compiles all test circuits on arrays up to 64×64 qubits, circuit depth across configurations comparable to existing methods while dramatically reducing compilation time.

2. Related Works

2.1. Reconfigurable Neutral Atom Computing

Neutral atom quantum computing has attracted growing interest due to its advantages in large-scale quantum computation and inherent reconfigurability [13]. In reconfigurable neutral atom quantum computers, qubits are trapped within optical tweezers using two primary trap types: spatial light modulators (SLM) and crossed two-dimensional acousto-optic deflectors (AOD) [14]. The key distinction between these trap types lies in

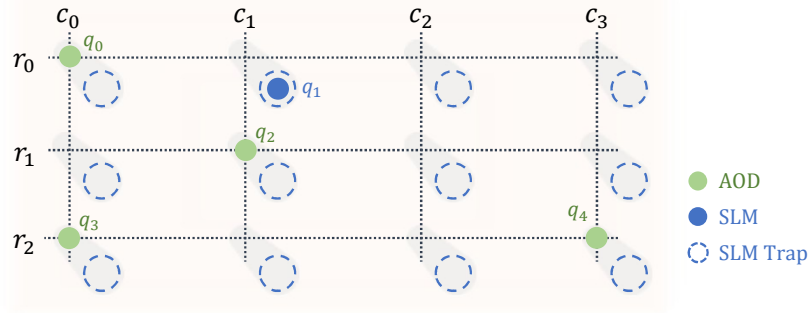


Figure 1: A reconfigurable atom array with AOD and SLM traps.

their mobility—SLM-generated traps remain fixed in position, whereas AOD-generated traps can be dynamically moved in space. When two atoms are brought sufficiently close, they can be illuminated by a Rydberg laser, enabling the execution of entangling gates. Intuitively, AOD traps function as “transporters” that shuttle atoms near other atoms with which they need to form entangling gates, thereby facilitating multi-qubit gate operations.

As shown in Fig. 1, in a reconfigurable neutral atom array with both AOD and SLM traps, qubits can reside in two types of traps simultaneously. The AOD trap forms a rectangular array with current implementations achieving 16×16 configurations [22], while the SLM trap can generate trapping sites at arbitrary positions within the plane. This arrangement enables flexible atomic repositioning, facilitating entanglement between different qubits and achieving enhanced connectivity and programmability.

However, the flexibility and reconfigurability that make neutral atom platforms attractive also create unique compilation challenges. The compilation process must account for hardware-specific constraints as follow:

- **AOD crossing constraint:** no two columns or rows within an AOD array may intersect.
- **Parallel execution constraint:** when two qubits undergo a two-qubit gate operation, no third qubit can be present within a certain vicinity.
- **Rydberg interaction constraint:** two qubits must be positioned within the Rydberg blockade radius r_b to enable entangling gate operations between them.

All neutral atom quantum computers must satisfy these hardware-specific requirements to function properly, representing universal challenges across this computing paradigm. As the technology advances, the solution space becomes dramatically expansive, creating a tension between compilation efficiency and hardware flexibility that must be resolved to fully exploit the potential of neutral atom quantum computing.

2.2. *Compilation for Reconfigurable Neutral Atom Arrays*

The physical constraints of reconfigurable neutral atom systems, particularly the AOD crossing constraint and parallel execution constraint, complicate the quantum compilation process. These constraints transform the compilation problem from a purely computational challenge into one that must deeply integrate hardware physics considerations. As noted in 2.1, the AOD crossing constraint prevents certain qubit movements, as they would require crossing AOD columns or rows. Meanwhile, the parallel execution constraint limits which gates can be executed simultaneously, as qubits involved in gate operations must maintain specific separation distances.

Fig. 1 illustrates a reconfigurable atom array architecture with both AOD and SLM traps represented on a coordinate grid. The horizontal axis (columns c_0, c_1, c_2, c_3) and vertical axis (rows r_0, r_1, r_2) form a coordinate system for precise qubit positioning. In this representation, AOD traps are depicted at grid intersections where vertical and horizontal acousto-optic deflectors meet, shown as solid circles. The SLM trap, on the other hand, can generate trapping sites at arbitrary positions within the plane. However to enhance parallelism, it is typically structured similarly to the AOD array, forming a rectangular grid [19]. Each quantum bit is assigned to a specific coordinate position, for example, qubit q_0 is positioned at the intersection of (r_0, c_0) in an AOD trap, while qubit q_1 is shown in an SLM trap. Here's an example to show how reconfigurable neutral atom array works.

In a reconfigurable neutral atom computer, qubits can move with AOD traps. But their movement is subject to constraints and the most critical being the AOD crossing constraint. Fig. 2 illustrates this constraint, which extracts a section of Fig. 1, highlighting two vertically and two horizontally oriented acousto-optic deflectors. If qubit q_0 at (r_0, c_0) needs to establish entanglement with qubit q_1 in the SLM trap, directly moving q_0 to q_1 is prohibited, as it would cause column c_0 to cross over column c_1 , violating the AOD crossing constraint.

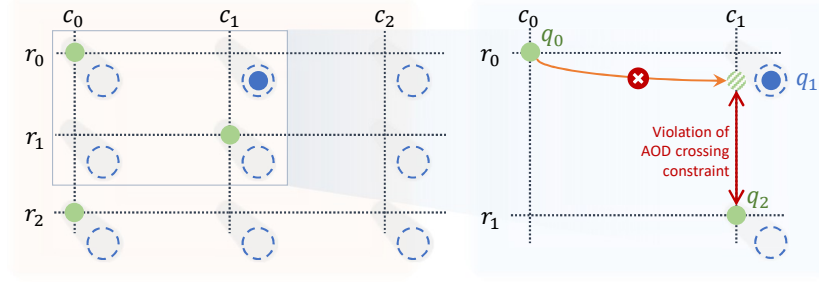


Figure 2: Illustration of AOD crossing constraint violation.

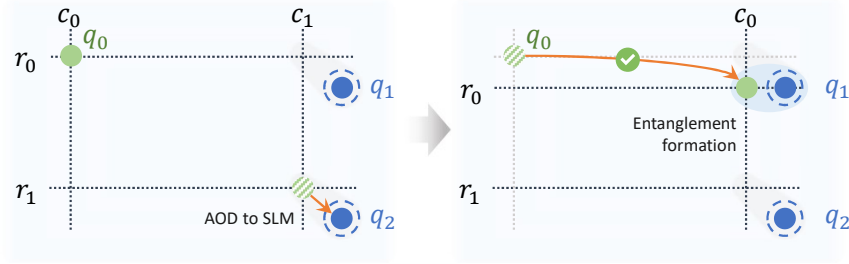


Figure 3: Qubit transition from AOD to SLM trap for entanglement formation.

To address this issue, one approach is illustrated in Fig. 3, where qubit q_2 is relocated to an SLM trap to avoid AOD crossing. This transition from an AOD trap to an SLM trap can be achieved by reducing the intensity of the AOD trap while either enhancing or maintaining the intensity of the SLM trap. After this operation, q_2 in the SLM trap no longer requires vertical or horizontal acousto-optic deflectors to maintain its position. Next, within the AOD array, c_0 is shifted rightward, and r_0 is moved downward, allowing q_0 to be transported near q_1 at a distance smaller than the Rydberg blockade radius r_b . At this point, q_0 and q_1 can form an entanglement gate.

Notably, as long as the row/column non-crossing constraint of the AOD array is maintained, different sections of the array can operate independently. This characteristic enables neutral atom quantum computing with significant flexibility and reconfigurability. In addition to the AOD crossing constraint, neutral atom quantum computers must also adhere to the parallel execution constraint, which dictates that when two qubits undergo a two-qubit gate operation, no third qubit can be present within a certain vicinity determined by the Rydberg blockade radius r_b [19, 17].

Table 1: Compilation time of DPQA.

Quantum Circuit	Qubits	Gates	Depth	Compilation Time(s)
rand3reg_70_0	70	105	15	2906.7
rand3reg_70_1	70	105	12	3195.9
rand3reg_70_2	70	105	14	3573.4
rand3reg_70_3	70	105	14	3312.3
rand3reg_70_4	70	105	15	2848.3
rand3reg_80_3	70	105	12	9696.3
rand3reg_80_4	70	105	14	8088.4
rand3reg_80_7	70	105	16	8756.2
rand3reg_80_8	70	105	18	9334.1
rand3reg_80_9	70	105	15	9630.4

2.3. Related work

To effectively address these constraints and establish a well-defined compilation process for reconfigurable neutral atom arrays, several methods have been proposed. Tan et al. [19] first discretized the working space of the quantum compilation problem by partitioning space into an array of sites that are sufficiently spaced apart and restricting quantum gate execution to operate in a single site. This approach effectively mitigates issues arising from the restriction zone. Based on this architecture, they also introduced the first solver-based compilation method for reconfigurable neutral atom arrays. Building upon this work, Tan et al. [20] proposed DPQA, a compilation method that integrates a greedy search algorithm with solver-based approaches to improve both computational efficiency and scalability. This method enhances the scalability of the original solver-based approach, further optimizing the compilation of reconfigurable neutral atom quantum circuits.

Although DPQA significantly accelerates the compilation process for neutral atom quantum computers, it still suffers from severe computational efficiency issues. The compilation times for 10 circuits containing 70 to 80 qubits, as shown in Table 1, range from approximately 2848 seconds to over 9600 seconds. Such excessive compilation times lead to inefficient utilization of quantum computing resources, which is an increasingly pressing concern as quantum circuits continue to grow in size. Furthermore, as neutral atom quantum computer technology advances, the solution space for neutral quantum compilation becomes dramatically expansive with the increasing scale of 2D arrays, and current neutral atom compilation techniques still exhibit significant limitations in addressing this challenge.

3. Physics-Aware Compilation for Parallel Quantum Circuit Execution

3.1. Key issues and methods overviews

In the field of neutral atom quantum compilation, various methods have been proposed to address hardware-specific constraints. Among these approaches, solver-based methods have demonstrated significantly better results compared to heuristic approaches, making them widely adopted in practical applications. However, since the solver is based on the Max-SAT problem which is NP-Hard [23], solver efficiency represents a critical challenge in these methods. As shown in Table 1, compilation times for moderately complex circuits can reach thousands of seconds, imposing prohibitive computational costs that become increasingly severe with larger system sizes. Combined with the flexibility of neutral atom hardware, this leads to a technical tension where maintaining the inherent reconfigurability of these systems while achieving acceptable compilation performance becomes challenging. To fully leverage the advantages of neutral atom quantum computers, more efficient approaches are needed that preserve hardware flexibility while delivering practical compilation times.

We also observe that applying solvers across the entire computational plane creates unnecessary coupling between regions that could be processed independently. This superfluous coupling reduces compilation efficiency by preventing naturally separable quantum operations from being executed in parallel, despite the inherent physical independence provided by the quantum hardware architecture.

Our analysis suggests an alternative approach that integrates hardware physics understanding into the compilation process. Rather than treating compilation as purely computational, we recognize that the physical characteristics of neutral atom hardware provide natural opportunities for problem decomposition. The physical constraints of neutral atom arrays create natural boundaries that can be leveraged to partition both the hardware plane and the quantum circuit, reducing the solution space without sacrificing hardware flexibility.

Based on these insights, we propose Physics-Aware Compilation (PAC), a method that addresses these challenges by integrating hardware physics into the compilation process. As shown in Fig. 4, PAC consists of two sequential components:

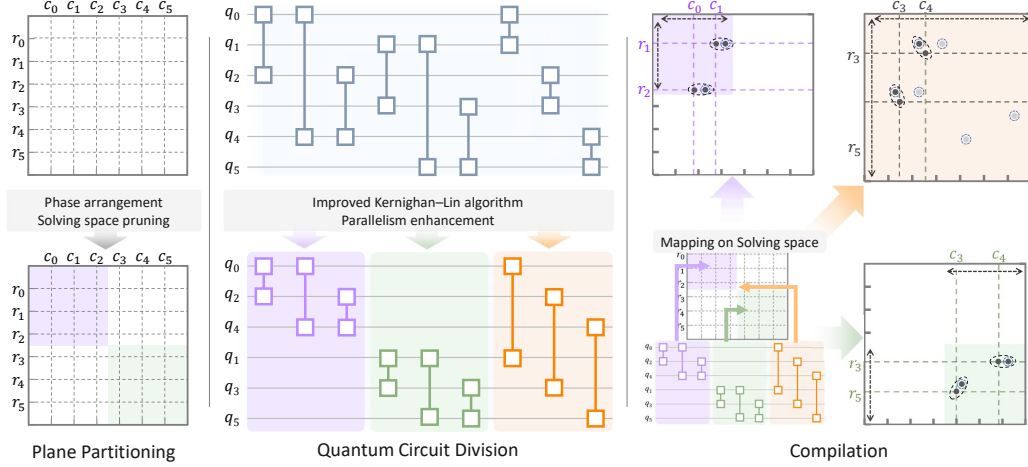


Figure 4: Workflow of PAC.

- **Hardware Plane Partitioning** divides the 2D hardware plane into independent sections based on physical device characteristics. This partitioning leverages the natural boundaries created by physical constraints to reduce the solution space while enabling parallelism in the compilation process.
- **Quantum Circuit Division** transforms the quantum circuit compilation problem through an improved graph-based partitioning approach. By dividing the circuit into communities with stronger internal connections, this component enables more efficient compilation by aligning with the underlying physical structure of quantum operations.

These techniques work together to improve compilation efficiency while preserving the hardware flexibility that makes neutral atom platforms more attractive for quantum computing applications.

3.2. Hardware Plane Partitioning

Hardware plane partitioning is demonstrated using a 6×6 neutral atom array in Fig.5, addressing efficiency challenges through strategic resource division. The process comprises two sequential phases: local and global, operating on the target quantum circuit.

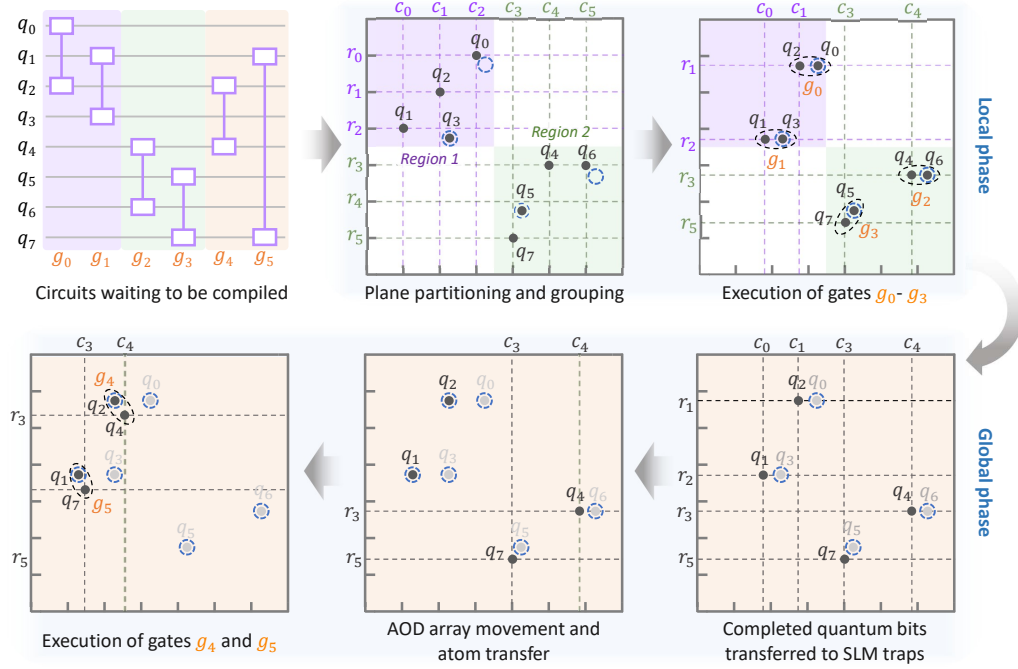


Figure 5: Demonstration of hardware plane partitioning.

In the local phase, we partition the hardware plane into two equal-sized regions, as shown in Figure 5: Region 1 (purple, upper left) and Region 2 (green, lower right). The AOD array is similarly divided into two groups: the first includes columns c_0, c_1, c_2 and rows r_0, r_1, r_2 , while the second includes columns c_3, c_4, c_5 and rows r_3, r_4, r_5 . This partitioning leverages a key physical property of the hardware: AOD arrays in separate regions can operate independently without interference, enabling true parallelism in the compilation process. During this phase, we perform initial mapping by dividing the logical qubits between the two regions and then compile all quantum operations that can be executed entirely within either region like $g_0 - g_3$.

During compilation, we classify qubits in each region into two types based on their interaction in quantum circuit: resolved qubits and active qubits. Resolved qubits (such as q_0, q_3, q_5 and q_6 in Figure 5) can complete all their required operations entirely within their assigned region during the local phase. Active qubits (q_1, q_2, q_4 and q_7) require interactions with qubits in other regions and therefore need additional operations in the global phase to complete their quantum gates.

Global phase compilation requires all resolved qubits to be placed in SLM traps by the local phase conclusion, as shown in Figure 5 where resolved qubits appear in gray. This arrangement is critical: SLM traps do not occupy AOD grid positions, enabling active qubits to move freely during the global phase without obstruction. This requirement is implemented through appropriate constraints in the local phase compilation. The global phase inherits qubit positions and states from the local phase as initial conditions, then completes compilation by processing remaining operations across the entire plane. By focusing exclusively on active qubits and their cross-region interactions, this approach reduces problem complexity compared to traditional methods that process all qubits simultaneously. The final compilation solution merges both phases' results, with total circuit depth calculated as the maximum depth between the two local phases plus the depth of the global phase. Algorithm 1 presents the complete hardware plane partitioning process as follow.

Algorithm 1: Hardware Plane Partitioning

Input: A $N \times N$ Neutral Atom Array A , A Commutable Quantum Circuit

$$QC = \{Q, E\}$$

Output: Compilation result R

// Partition the hardware plane into two sub-arrays

$$A_1 = A[0 : \lceil \frac{N}{2} \rceil - 1, 0 : \lceil \frac{N}{2} \rceil - 1];$$

$$A_2 = A[\lceil \frac{N}{2} \rceil : N, \lceil \frac{N}{2} \rceil : N];$$

// Decompose QC into three subcircuits:

$$QC_1 = (Q_1, E_1), QC_2 = (Q_2, E_2), QC_3 = (Q_3, E_3), Q_{a1}, Q_{a2} \leftarrow \text{Partition}(QC)$$

$$\text{where } Q_{a1} = Q_1 \setminus Q(E_3), Q_{a2} = Q_2 \setminus Q(E_3);$$

// Local Phase Compilation

$R_1 \leftarrow \text{Compile}(QC_1, A_1)$, with all Q_{a1} qubits placed in SLM traps in the last layer;

$R_2 \leftarrow \text{Compile}(QC_2, A_2)$, with all Q_{a2} qubits placed in SLM traps in the last layer;

// Global Phase Compilation

for $q \in Q$ **do**

 Retrieve q 's state and position from A ;

 Update R_1 and R_2 accordingly;

end

$R_3 \leftarrow \text{Compile}(QC_3, A)$, inheriting qubit states and positions from R_1 and R_2 ;

// Merge results

$R \leftarrow \text{Merge}(R_1, R_2, R_3)$; Return R ;

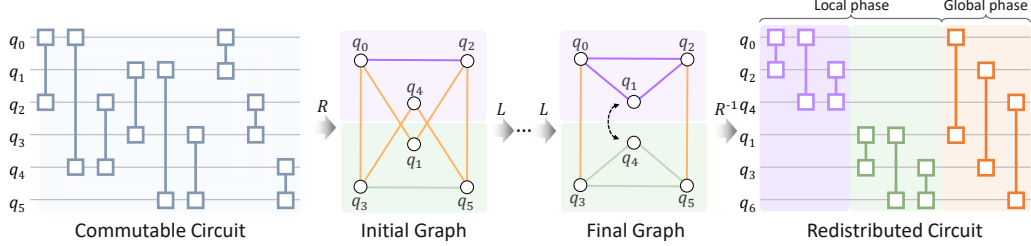


Figure 6: Demonstration of quantum circuit division.

The efficiency advantage of hardware plane partitioning stems from two intuitive but effective key factors. First, hardware-level partitioning significantly prunes the solution space by reducing the number of variables and constraints that must be handled by the solver in each phase. Instead of solving one large optimization problem across the entire hardware plane, we solve multiple smaller problems that are computationally more tractable. Second, the independence of regions in the local phase enables parallel compilation, further reducing the overall time required.

3.3. Quantum Circuit Division

Quantum circuit division addresses the second key component of our physics-aware approach, focusing on how to effectively partition quantum operations to maximize parallel execution capabilities. The goal is to determine which gates should be executed in the local phase versus the global phase to minimize overall compilation time, defined as $T = T_1 + T_2$, where T_1 and T_2 correspond to the compilation time for the local and global phases, respectively. With N_G total quantum gates requiring compilation, this becomes an allocation problem of distributing gates between phases. Since the hardware plane partitioning enables parallel execution in the local phase with reduced search space, strategies for component prioritizes maximizing the number of gates assigned to the local phase while minimizing cross-region interactions that must be handled in the global phase.

To achieve effective quantum circuit division, we propose an improved Kernighan–Lin algorithm that aligns with the physical structure of the neutral atom hardware. As illustrated in Fig. 6, algorithm begins by representing the quantum circuit as a graph where each qubit corresponds to a vertex and each two-qubit gate corresponds to an edge. This graph representation

naturally captures the physical interaction patterns between qubits. The vertices are then evenly partitioned into two communities, corresponding to the two regions of the hardware plane. Within each community, qubits are classified into resolved qubits and active qubits as previously defined in Section 3.2. The process determine resolved qubits and active qubits is shown in Algorithm 2 as follow.

Algorithm 2: Identify initial resolved qubits and active qubits

Input: A Commutable Quantum Circuit $QC = \{Q, E\}$, Weight parameter k ,

Maximum number of swaps Max_iter

Output: Quantum circuit partitions for local and global phase compilation

QC_1, QC_2, QC_3

$Q_1 = \text{RandomSubset}(Q, \lceil |Q|/2 \rceil)$;

$Q_2 = Q \setminus Q_1$;

$swap_flag = \text{True}$;

$n_iter = 0$;

$E_1, E_2, E_3 = \{\}, \{\}, \{\}$;

Active qubits $Q_{a1}, Q_{a2} = \{\}, \{\}$;

for e **in** E **do**

if $e[0]$ **in** Q_1 **and** $e[1]$ **in** Q_1 **then**

$E_1 = E_1 \cup \{e\}$;

else if $e[0]$ **in** Q_2 **and** $e[1]$ **in** Q_2 **then**

$E_2 = E_2 \cup \{e\}$;

else if $e[0]$ **in** Q_1 **and** $e[1]$ **in** Q_2 **then**

$E_3 = E_3 \cup \{e\}$;

else if $e[0]$ **in** Q_1 **and** $e[1]$ **in** Q_2 **then**

$E_3 = E_3 \cup \{e\}$;

$Q_{a1} \cup \{e[0]\}$;

$\cup Q_{a2} \cup \{e[1]\}$;

else if $e[0]$ **in** Q_2 **and** $e[1]$ **in** Q_1 **then**

$E_3 = E_3 \cup \{e\}$;

$Q_{a1} \cup \{e[1]\}$;

$Q_{a2} \cup \{e[0]\}$;

end

end

$Q_{r1} = Q_1 \setminus Q_{a1}$;

$Q_{r2} = Q_2 \setminus Q_{a2}$;

return Resolved qubits Q_{r1}, Q_{r2} , Active qubits Q_{a1}, Q_{a2} , Edge sets E_1, E_2, E_3

Next, candidates for community reassignment are identified by examining active qubits’ connectivity patterns. Qubits with more external connections than internal ones are defined as swap qubits, indicating suboptimal placement from a physical execution perspective, since they interact more with qubits outside their region than within it. If one community has no swap qubits while another does, active qubits from the empty-set community are designated as swap qubits to enable balanced optimization.

We then iteratively optimize the community structure by swapping pairs of swap qubits between communities, computing the loss function L for each potential swap. This process directly improves the physical execution efficiency by minimizing cross-region interactions that would require more complex global phase compilation. The pair of qubits that minimizes L is selected for swapping, followed by an update of resolved and active qubit classifications. This optimization process continues until one of three termination conditions is met: (a) both communities have empty swap qubit sets, indicating an optimal or near-optimal partition has been achieved; (b) the number of swaps reaches a predefined upper limit to prevent excessive computation; (c) no swap operation can further reduce the loss function L , suggesting we’ve reached a local optimum in the partition quality.

The loss function L is defined as:

$$L = k(N_{f,1} + N_{f,2}) + (1 - k)(N_{E,cross}) \quad (1)$$

Here, N_{f1} and N_{f2} represent the number of active qubits in each of the two communities that require cross-region interactions, while $N_{E,cross}$ denotes the number of edges (two-qubit gates) between these communities. The parameter $k \in [0, 1]$ balances the optimization priority between minimizing active qubits and minimizing cross-region gates. This physics-aware loss function directly targets the efficiency bottleneck: by minimizing L , we reduce both the number of qubits and the number of gates that must be processed in the computationally expensive global phase, thereby maximizing the operations that can be executed in parallel during the local phase.

After optimization, we convert the resulting graph back into a quantum circuit and mark each gate for execution in either the local or global phase based on the final community structure. This physics-guided partitioning transforms the conventional global compilation problem into a more efficient region-based approach. The improved Kernighan–Lin algorithm is shown in Algorithm 3.

Algorithm 3: The improved Kernighan–Lin algorithm

Input: A Commutable Quantum Circuit $QC = \{Q, E\}$, Resolved qubits Q_{r1} , Q_{r2} , Active qubits Q_{a1} , Q_{a2} , Edge sets E_1 , E_2 , E_3 , Weight parameter k , Maximum number of swaps Max_iter

Output: Quantum circuit partitions QC_1 , QC_2 , QC_3

$swap_flag = \text{True}$;

$n_iter = 0$;

$swap_flag = \text{False}$;

while True **do**

 // Identify swap qubits

$Q_{s1}, Q_{s2} = \{\}, \{\}$;

for q **in** Q_{a1} **do**

if $|\{e \in E_3 | q \in e\}| \leq |\{e \in E_1 | q \in e\}|$ **then**

$Q_{s1} \cup \{q\}$;

end

end

for q **in** Q_{a2} **do**

if $|\{e \in E_3 | q \in e\}| \leq |\{e \in E_2 | q \in e\}|$ **then**

$Q_{s2} \cup \{q\}$;

end

end

if $Q_{s1} == \{\}$ **then**

$Q_{s1} = Q_{a1}$;

end

if $Q_{s2} == \{\}$ **then**

$Q_{s2} = Q_{a2}$;

end

$min_L = k(|Q_{a1}| + |Q_{a2}|) + (1 - k)|E_3|$;

$best_q1, best_q2 = \text{None}, \text{None}$;

for each $(q_1, q_2) \in Q_{s1} \times Q_{s2}$ **do**

 Try swap $q_1, q_2 \Rightarrow$ and compute L ;

if $L \leq min_L$ **then**

$best_q1, best_q2 = q_1, q_2$;

$min_L = L$;

end

end

if $best_q1$ is not None and $best_q2$ is not None **then**

 Swap $best_q1$ and $best_q2$;

$swap_flag = \text{True}$;

$n_iter = n_iter + 1$;

end

if $(Q_{s1} == \{\} \text{ and } Q_{s2} == \{\})$ or not $swap_flag$ or $n_iter \leq Max_iter$ **then**

break;

end

end

return $QC_1 = (Q_1, E_1)$, $QC_2 = (Q_2, E_2)$, $QC_3 = (Q_3, E_3)$, Q_{a1} , Q_{a2} , Q_{r1} , Q_{r2}

At this stage, the quantum circuit is partitioned into three segments: QC_1 , QC_2 , and QC_3 . The qubits involved in QC_1 and QC_2 are categorized into active qubits (Qa_1, Qa_2) and resolved qubits (Qr_1, Qr_2). According to the hardware plane partitioning strategy, QC_1 and QC_2 are executed in the local phase, while QC_3 is assigned to the global phase. As described in Section 3.2, the local phase serves as the initial stage of solving, where QC_1 and QC_2 are processed in parallel.

To prevent interference from resolved qubits in the local phase during the subsequent global phase, we impose specific constraints during local-phase solving. To clearly illustrate our method, we adopt the same variable definitions as DPQA[20]. Specifically, we define $x_{i,t}$ and $y_{i,t}$ as the SLM coordinates of qubit i at time t , while $c_{i,t}$ and $r_{i,t}$ denote the corresponding AOD column and row indices. The binary variable $a_{i,t}$ indicates the state of qubit i at time t , where $a = 0$ represents the SLM state and $a = 1$ represents the AOD state.

In the local phase, if all remaining gates are resolved at a given solving step, we impose the following constraint on all resolved qubits to avoid unnecessary interaction in the global phase:

$$\forall i \in Q_{r1}, \forall t, \text{ if } t \text{ is the final stage, } a_{i,t} = 0 \quad (2)$$

The above constraint effectively prevents resolved qubits from interfering with the global phase and reduces the number of variables involved in global-phase solving.

In the global phase, QC_3 is solved over the entire neutral atom array. To ensure continuity and reduce the solution space, we introduce two additional constraints. First, since each SLM trap can accommodate at most one atom, no qubit in the global phase is allowed to occupy an SLM position already assigned to a qubit in the local phase:

$$\forall t, \forall (x_s, y_s) \in \mathcal{F}, \quad \neg(x_{i,t} = x_s \wedge y_{i,t} = y_s \wedge a_{i,t} = 0) \quad (3)$$

where \mathcal{F} denotes the set of SLM coordinates of Q_{r1} and Q_{r2} in the local phase. To ensure consistency between the local phase and the global phase, the initial configuration of the global phase must satisfy the final state of the local phase, including both SLM and AOD assignments. The SLM coordinates of each qubit in the global phase must match its final position in the local phase. Let (x_q^L, y_q^L) denote the final SLM coordinates of qubit q in active qubits of local phase. Then:

$$x_{q,0} = x_q^L \wedge y_{q,0} = y_q^L, \quad \forall q \in Q_{a1} \cup Q_{a2} \quad (4)$$

The AOD channel assignment in the global phase must preserve the relative ordering of qubits established in the local phase. Let c_q^L represent the final AOD index of qubit q in the local phase, and $c_{q,0}$ its AOD index at time $t = 0$ in the global phase. Then, for any pair of qubits $q_1, q_2 \in Q_{a1} \cup Q_{a2}$, the following conditions must hold:

$$\begin{cases} c_{q_1,0} < c_{q_2,0}, & \text{if } c_{q_1}^L < c_{q_2}^L \\ c_{q_1,0} > c_{q_2,0}, & \text{if } c_{q_1}^L > c_{q_2}^L \\ c_{q_1,0} = c_{q_2,0}, & \text{if } c_{q_1}^L = c_{q_2}^L \end{cases} \quad \text{for all } q_1, q_2 \in Q_{a1} \cap Q_{a2} \quad (5)$$

These constraints are essential to guarantee the correctness of the compilation process and to ensure seamless continuity between the local and global phases.

4. Experimental Results

4.1. Experimental Setup

PAC was evaluated against DPQA [20], the current state-of-the-art method for neutral atom quantum compilation. DPQA has demonstrated performance improvements over previous approaches such as RAA [19], making it an appropriate baseline for comparison. The evaluation utilized 40 random 3-regular graph circuits with 60 – 90 qubits and 90 – 135 two-qubit gates, identical to those used in DPQA’s evaluation. These circuits are applicable to various combinatorial optimization problems including Max-Cut and quantum simulation algorithms such as QAOA and trotterized adiabatic evolution [24, 25]. To assess scalability, performance was tested across multiple neutral atom array dimensions: 16×16 , 20×20 , 24×24 , 28×28 , 50×50 , and 64×64 . The 16×16 configuration represents currently proposed experimental systems, while larger dimensions reflect anticipated future hardware capabilities. Performance was measured using two key metrics: compilation efficiency through solution time and speedup ratio compared to baseline with a 10,000-second timeout threshold, and compilation quality through quantum circuit layer count and layer reduction ratio defined as follow:

$$R_{cl} = \frac{NL_{PAC} - NL_{baseline}}{NL_{baseline}} \quad (6)$$

where NL_{PAC} and $NL_{baseline}$ are number of circuit layers after PAC and baseline, respectively. Detailed information about the experimental setup is provided in Appendix B.

4.2. Solving Efficiency and Quality

Table 2 presents the compilation performance comparison between PAC and DPQA on a 16×16 AOD array. PAC demonstrates substantial efficiency improvements, compiling all test circuits within 1200 seconds, while DPQA encounters limitations when dealing with circuits beyond 70 qubits. For circuits where both methods complete, PAC shows a notable speedup of up to $78.5\times$ with an average acceleration of $53.5\times$, corresponding to a significant reduction in compilation time. Importantly, this performance gain does not compromise compilation quality, as PAC maintains an average circuit depth of 12.6, comparable to DPQA’s results across most circuits.

The performance advantage becomes more pronounced on larger architectures, as shown in Table 3 for a 64×64 array. On this larger configuration, PAC achieves even greater efficiency with a peak speeds up to $139.16\times$ and completes all test circuits in under 200 seconds. The average speedup across DPQA-solvable circuits increases to $78.23\times$. Despite this substantial acceleration, PAC maintains high-quality results with an average circuit depth of 12.76 compared to DPQA’s 12.8, demonstrating that the performance improvements do not come at the expense of compilation quality.

A clear trend emerges when examining PAC’s performance across different array sizes: compilation efficiency improves as hardware scale increases. While maximum compilation time reaches approximately 1200 seconds on 16×16 arrays, it decreases to under 200 seconds on 64×64 arrays, indicating excellent scalability with hardware size. This positive scaling relationship suggests that PAC’s advantage becomes more valuable as quantum hardware continues to advance toward larger scales. Results for intermediate array sizes (20×20 , 24×24 , 28×28 , and 50×50) follow the same trend and are presented in Appendix C.

Table 2: Solving Time and Circuit Layers on 16×16 Array.

Quantum Circuit	Qubits	Solving time (s)			Circuit Layers			
		DPQA	PAC	Speedup	DPQA	PAC	Δ_{cl}	R_{cl}
rand3reg_60_0	60	1728.42	30.40	56.86 ↑	12	13	1	8.33%
rand3reg_60_1	60	2701.22	39.99	67.54 ↑	11	12	1	9.09%
rand3reg_60_2	60	1281.69	50.71	25.27 ↑	10	11	1	10.00%
rand3reg_60_3	60	1968.34	35.16	55.98 ↑	10	11	1	10.00%
rand3reg_60_4	60	1817.24	30.81	58.98 ↑	12	12	0	0.00%
rand3reg_60_5	60	1420.21	48.28	29.41 ↑	12	12	0	0.00%
rand3reg_60_6	60	1645.56	48.93	33.63 ↑	12	12	0	0.00%
rand3reg_60_7	60	1636.04	37.72	43.38 ↑	10	11	1	10.00%
rand3reg_60_8	60	1871.13	35.61	52.55 ↑	11	12	1	9.09%
rand3reg_60_9	60	1853.53	40.75	45.49 ↑	13	13	0	0.00%
rand3reg_70_0	70	5539.06	75.14	73.72 ↑	13	13	0	0.00%
rand3reg_70_1	70	5746.01	139.23	41.27 ↑	12	12	0	0.00%
rand3reg_70_2	70	4353.12	82.84	52.55 ↑	13	13	0	0.00%
rand3reg_70_3	70	6270.31	97.65	64.21 ↑	13	14	1	7.69%
rand3reg_70_4	70	6873.92	117.21	58.64 ↑	12	12	0	0.00%
rand3reg_70_5	70	5999.32	76.40	78.52 ↑	14	14	0	0.00%
rand3reg_70_6	70	6334.61	87.66	72.27 ↑	13	14	1	7.69%
rand3reg_70_7	70	6214.34	137.41	45.22 ↑	12	14	2	16.67%
rand3reg_70_8	70	6179.55	97.32	63.50 ↑	14	14	0	0.00%
rand3reg_70_9	70	3847.52	75.23	51.15 ↑	11	13	2	18.18%
rand3reg_80_0	80	TO	559.48	> 17.87 ↑	-	15	-	-
rand3reg_80_1	80	TO	239.20	> 41.81 ↑	-	15	-	-
rand3reg_80_2	80	TO	360.70	> 27.72 ↑	-	15	-	-
rand3reg_80_3	80	TO	964.44	> 10.37 ↑	-	15	-	-
rand3reg_80_4	80	TO	277.58	> 36.03 ↑	-	14	-	-
rand3reg_80_5	80	TO	769.42	> 13.00 ↑	-	15	-	-
rand3reg_80_6	80	TO	287.65	> 34.76 ↑	-	15	-	-
rand3reg_80_7	80	TO	152.97	> 65.37 ↑	-	14	-	-
rand3reg_80_8	80	TO	545.00	> 18.35 ↑	-	15	-	-
rand3reg_80_9	80	TO	341.63	> 29.27 ↑	-	15	-	-
rand3reg_90_0	90	TO	674.18	> 14.83 ↑	-	16	-	-
rand3reg_90_1	90	TO	561.58	> 17.81 ↑	-	16	-	-
rand3reg_90_2	90	TO	784.85	> 12.74 ↑	-	18	-	-
rand3reg_90_3	90	TO	668.09	> 14.97 ↑	-	18	-	-
rand3reg_90_4	90	TO	583.63	> 17.13 ↑	-	18	-	-
rand3reg_90_5	90	TO	642.10	> 15.57 ↑	-	16	-	-
rand3reg_90_6	90	TO	1164.81	> 8.59 ↑	-	20	-	-
rand3reg_90_7	90	TO	455.63	> 21.95 ↑	-	18	-	-
rand3reg_90_8	90	TO	671.65	> 14.89 ↑	-	18	-	-
rand3reg_90_9	90	TO	903.11	> 11.07 ↑	-	18	-	-
		3764.06	69.22	53.51 ↑	12	12.6	0.6	5.00%

Table 3: Solving Time and Circuit Layers on 64×64 Array.

Quantum Circuit	Qubits	Solving time (s)			Circuit Layers			
		DPQA	PAC	Speedup	DPQA	PAC	Δ_{cl}	R_{cl}
rand3reg_60_0	60	1316.52	18.19	72.37 ↑	12	11	-1	-8.33%
rand3reg_60_1	60	1040.71	23.62	44.06 ↑	12	12	0	0.00%
rand3reg_60_2	60	1411.00	22.56	62.55 ↑	11	11	0	0.00%
rand3reg_60_3	60	1528.79	24.22	63.13 ↑	12	12	0	0.00%
rand3reg_60_4	60	892.77	18.01	49.56 ↑	11	10	-1	-9.09%
rand3reg_60_5	60	1525.45	22.12	68.96 ↑	12	12	0	0.00%
rand3reg_60_6	60	953.52	20.08	47.47 ↑	12	12	0	0.00%
rand3reg_60_7	60	1337.51	21.76	61.45 ↑	11	12	1	9.09%
rand3reg_60_8	60	1070.16	19.12	55.98 ↑	11	11	0	0.00%
rand3reg_60_9	60	873.20	22.11	39.49 ↑	12	12	0	0.00%
rand3reg_70_0	70	2906.76	41.35	70.29 ↑	13	13	0	0.00%
rand3reg_70_1	70	3195.99	47.87	66.76 ↑	13	13	0	0.00%
rand3reg_70_2	70	3573.35	43.42	82.31 ↑	13	13	0	0.00%
rand3reg_70_3	70	3312.31	36.53	90.68 ↑	14	13	-1	-7.14%
rand3reg_70_4	70	2848.27	41.55	68.56 ↑	13	13	0	0.00%
rand3reg_70_5	70	3317.86	51.91	63.92 ↑	13	14	1	7.69%
rand3reg_70_6	70	4513.51	48.15	93.74 ↑	14	14	0	0.00%
rand3reg_70_7	70	3490.30	37.27	93.65 ↑	13	13	0	0.00%
rand3reg_70_8	70	3160.43	46.47	68.01 ↑	13	13	0	0.00%
rand3reg_70_9	70	3753.55	47.61	78.83 ↑	15	14	-1	-6.67%
rand3reg_80_0	80	TO	91.67	>109.09 ↑	-	16	-	-
rand3reg_80_1	80	TO	84.20	>118.76 ↑	-	14	-	-
rand3reg_80_2	80	TO	105.30	>94.96 ↑	-	16	-	-
rand3reg_80_3	80	9696.31	82.12	118.08 ↑	15	15	0	0.00%
rand3reg_80_4	80	8088.37	73.03	110.76 ↑	13	14	1	7.69%
rand3reg_80_5	80	TO	78.26	>127.78 ↑	-	14	-	-
rand3reg_80_6	80	TO	92.69	>107.88 ↑	-	14	-	-
rand3reg_80_7	80	8756.19	76.86	113.92 ↑	14	15	1	7.14%
rand3reg_80_8	80	9334.07	67.08	139.16 ↑	14	13	-1	-7.14%
rand3reg_80_9	80	9630.43	72.94	132.03 ↑	14	14	0	0.00%
rand3reg_90_0	90	TO	161.38	>61.97 ↑	-	16	-	-
rand3reg_90_1	90	TO	176.92	>56.52 ↑	-	17	-	-
rand3reg_90_2	90	TO	161.42	>61.95 ↑	-	17	-	-
rand3reg_90_3	90	TO	164.89	>60.65 ↑	-	16	-	-
rand3reg_90_4	90	TO	170.63	>58.61 ↑	-	16	-	-
rand3reg_90_5	90	TO	144.06	>69.42 ↑	-	16	-	-
rand3reg_90_6	90	TO	162.69	>61.47 ↑	-	17	-	-
rand3reg_90_7	90	TO	196.55	>50.88 ↑	-	17	-	-
rand3reg_90_8	90	TO	179.23	>55.79 ↑	-	17	-	-
rand3reg_90_9	90	TO	157.62	>63.44 ↑	-	17	-	-
		3661.09	41.04	78.23 ↑	12.8	12.76	-0.04	-0.31%

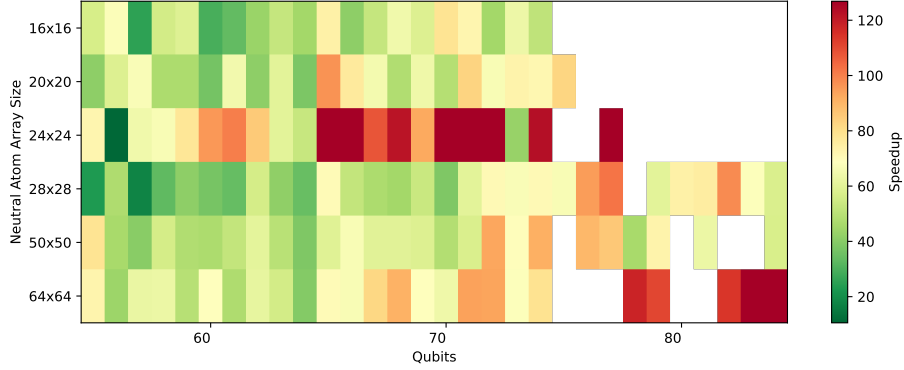


Figure 7: Heatmap visualization of PAC speedup factors relative to DPQA across varying qubit counts (60 – 80) and neutral atom array dimensions. White cells indicate instances where DPQA exceeded the computation time threshold, while color intensity corresponds to speedup magnitude. Each qubit count category includes ten benchmark circuits include *rand3reg-60_0* through *rand3reg-60_9*, *rand3reg-70_0* through *rand3reg-70_9*, and *rand3reg-80_0* through *rand3reg-80_9*.

To better understand PAC’s performance characteristics, Figure 7 presents a heatmap illustrating the speedup of PAC over DPQA across different qubit counts and neutral atom array sizes.

The visualization shows that speedup factors generally increase with qubit count, indicating better relative performance on larger problem sizes. The 24×24 array configuration exhibits higher acceleration ratios compared to other array sizes for equivalent circuits.

The contribution of the quantum circuit division component can be observed through the ablation experiment in Figure 8.

As the division process progresses, the number of edges between communities and the number of qubits requiring global phase compilation both decrease. This reduction in cross-region operations correlates with improved compilation efficiency, as shown by the downward trend in compilation time throughout the division process. The timing improvements confirm that the division strategy enhances local phase parallelism while reducing the computational load in the global phase.

Figure 9 illustrates the different scaling behaviors of both methods with increasing problem sizes.

DPQA’s solution time increases at a steeper rate with qubit count, while PAC shows a more moderate growth rate, especially for larger circuits. This

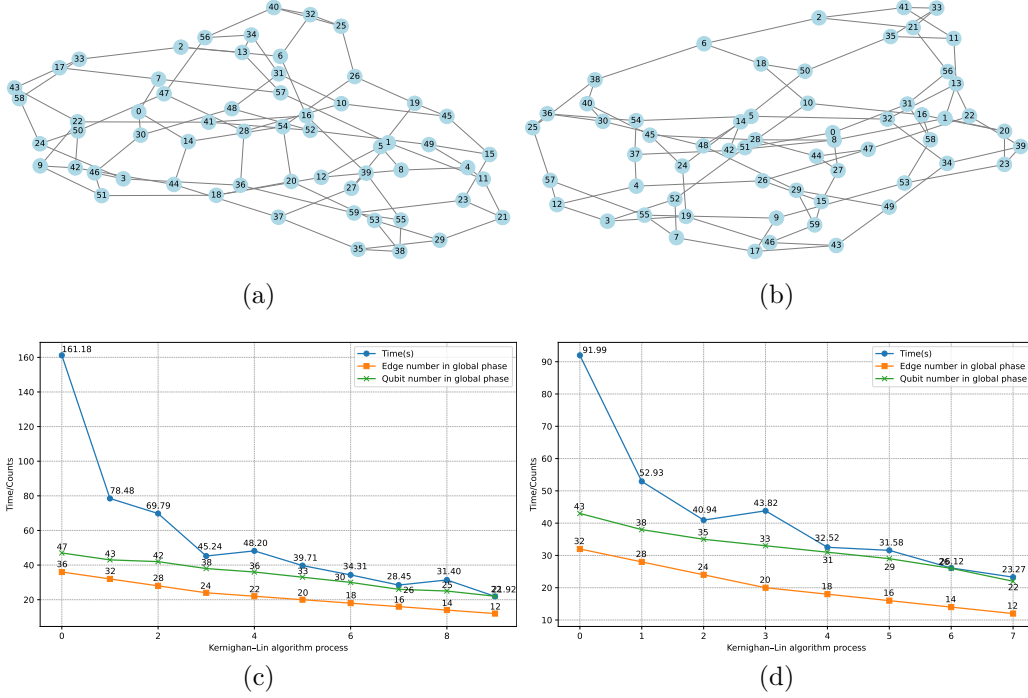


Figure 8: Ablation study of the Quantum Circuit Division process. (a) and (b) are two compiled 3-regular graph benchmarks, include *rand3reg-60_2* of 60 qubits and *rand3reg-60_9* of 90 edges. (c) and (d) represent the compilation metrics at progressive division stages for the corresponding benchmarks above. Blue lines represent compilation time, orange bars indicate the number of edges processed in the global phase, and blue-white bars show the number of qubits requiring global phase compilation.

difference in scaling patterns explains the widening performance gap observed in the earlier results and suggests that the physics-aware approach helps address efficiency limitations in conventional methods.

The analysis of these experimental results demonstrates that both Hardware Plane Partitioning and Quantum Circuit Division contribute to PAC’s performance improvements. By incorporating physical hardware characteristics into the compilation process, PAC achieves efficiency gains while maintaining compilation quality, offering a promising approach for neutral atom quantum computer compilation as hardware scales to larger dimensions.

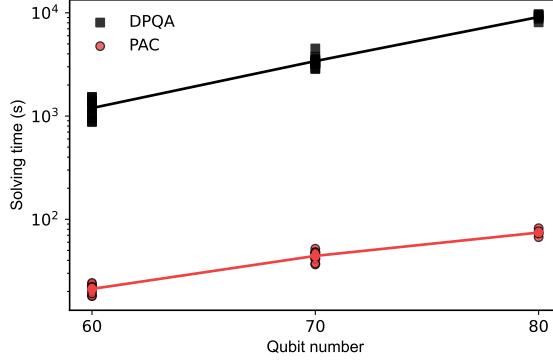


Figure 9: Comparison of compilation times between DPQA and PAC on a 64×64 neutral atom array, showing only circuits completed by DPQA within threshold. Data points represent individual circuits (DPQA: black squares; PAC: red circles), with logarithmic y-axis displaying performance scaling. Solid lines indicate mean compilation times per qubit count.

5. Discussion

Previous approaches to neutral atom quantum compilation have treated the problem primarily as computational, failing to effectively balance efficiency with hardware flexibility. PAC addresses this challenge by better leveraging the physical characteristics of quantum hardware, transforming the monolithic global problem into efficient local optimizations. This physics-aware approach achieved substantial performance improvements, with speedups of up to $78.5\times$ on 16×16 arrays and $139.16\times$ on 64×64 arrays compared to state-of-the-art methods, while maintaining comparable circuit quality. The increasing performance advantage at larger scales demonstrates PAC’s scalability, making PAC valuable as quantum systems continue to grow.

The current implementation has limitations that represent common challenges in neutral atom compilation. The approach primarily uses equal hardware plane division that may not be optimal for all circuit topologies. Future research could develop circuit-aware partitioning strategies that dynamically adjust boundaries based on circuit topologies and qubit interaction patterns, particularly for irregular or asymmetric structures. Additionally, considerations of fidelity variations across the hardware plane could be incorporated into the optimization process. Dynamic hardware constraint modeling could further enhance compilation, potentially enabling even more efficient utilization of promising quantum computing platforms.

6. Conclusion

In this work, we propose PAC, a physics-aware compilation framework for neutral atom quantum computers that balances compilation efficiency with hardware flexibility. This approach integrates hardware physics characteristics into the compilation process, decomposing the global problem into local optimizations through hardware plane partitioning and quantum circuit division. Experiments demonstrate PAC’s significant performance improvements across various array configurations while maintaining compilation quality.

Our exploration reveals two key insights into neutral atom quantum compilation. First, effectively exploiting the inherent parallelism of neutral atom architecture is crucial for improving compilation efficiency. The physical independence of different hardware regions creates natural opportunities for parallel processing that can be leveraged to reduce compilation time. Second, breaking down complex qubit mapping problems into simpler components through physics-guided partitioning transforms a challenging global optimization into more manageable sub-problems, improving efficiency while preserving solution quality.

Future work should focus on developing more adaptive physics-aware compilation strategies that can accommodate the diverse landscape of emerging quantum hardware architectures. Additionally, incorporating fidelity considerations into the compilation process would further leverage the unique advantages of neutral atom platforms, potentially enabling more robust quantum circuit execution as these systems scale toward practical quantum applications.

Authors’ contributions

Geng Chen: Writing - Original Draft, Visualization. **Guowu Yang:** Supervision, Formal analysis. **Wenjie Sun:** Methodology, Software. **Lianhui Yu:** Writing - Original Draft, Software. **Guangwei Deng:** Validation. **Desheng Zheng:** Methodology. **XiaoYu Li:** Conceptualization, Project administration.

Availability of supporting data

All data generated or analysed during this study are available and included in this published article. Code for our work has been open-sourced.

Acknowledgements

This work was supported by National Natural Science Foundation of China (Grant No. 62472072, No. 62172075 and No. U2441217), Natural Science Foundation of Xinjiang Uygur Autonomous Region (No. 2024D01A20), National Key Research and Development Program of China (No. 2022YFA1405900).

References

- [1] M. P. Harrigan, K. J. Sung, M. Neeley, K. J. Satzinger, F. Arute, K. Arya, J. Atalaya, J. C. Bardin, R. Barends, S. Boixo, et al., Quantum approximate optimization of non-planar graph problems on a planar superconducting processor, *Nature Physics* 17 (3) (2021) 332–336. doi:10.1038/s41567-020-01105-y.
URL <https://www.nature.com/articles/s41567-020-01105-y>
- [2] G. A. Quantum, Collaborators*†, F. Arute, K. Arya, R. Babbush, D. Bacon, J. C. Bardin, R. Barends, S. Boixo, M. Broughton, B. B. Buckley, et al., Hartree-Fock on a superconducting qubit quantum computer, *Science* 369 (6507) (2020) 1084–1089, publisher: American Association for the Advancement of Science. doi:10.1126/science.abb9811.
URL <https://www.science.org/doi/abs/10.1126/science.abb9811>
- [3] M. Cerezo, et al., Variational quantum algorithms, *Nature Reviews Physics* 3 (9) (2021) 625–644, publisher: Nature Publishing Group. doi:10.1038/s42254-021-00348-9.
URL <https://www.nature.com/articles/s42254-021-00348-9>
- [4] F. Arute, et al., Quantum supremacy using a programmable superconducting processor, *Nature* 574 (7779) (2019) 505–510, number: 7779 Publisher: Nature Publishing Group. doi:10.1038/s41586-019-1666-5.
URL <https://www.nature.com/articles/s41586-019-1666-5>
- [5] E. J. Thomas, V. N. Ciriano-Tejel, D. F. Wise, D. Prete, M. d. Kruijf, D. J. Ibberson, G. M. Noah, A. Gomez-Saiz, M. F. Gonzalez-Zalba, M. A. I. Johnson, J. J. L. Morton, Rapid cryogenic characterization of 1,024 integrated silicon quantum dot devices, *Nature Electronics* 8 (1) (2025) 75–83, publisher: Nature Publishing Group. doi:10.1038/s41928-024-01304-y.
URL <https://www.nature.com/articles/s41928-024-01304-y>
- [6] D. Bluvstein, et al., A quantum processor based on coherent transport of entangled atom arrays, *Nature* 604 (7906) (2022) 451–456, publisher: Nature

Publishing Group. doi:10.1038/s41586-022-04592-6.
URL <https://www.nature.com/articles/s41586-022-04592-6>

- [7] B. Tan, J. Cong, Optimal Layout Synthesis for Quantum Computing, in: 2020 IEEE/ACM International Conference On Computer Aided Design (ICCAD), 2020, pp. 1–9, iSSN: 1558-2434.
URL <https://ieeexplore.ieee.org/document/9256696>
- [8] B. Tan, J. Cong, Optimal qubit mapping with simultaneous gate absorption, in: 2021 IEEE/ACM International Conference On Computer Aided Design (ICCAD), 2021, pp. 1–8, iSSN: 1558-2434. doi:10.1109/ICCAD51958.2021.9643554.
URL <https://ieeexplore.ieee.org/document/9643554>
- [9] W.-H. Lin, J. Kimko, B. Tan, N. Bjørner, J. Cong, Scalable Optimal Layout Synthesis for NISQ Quantum Processors, in: 2023 60th ACM/IEEE Design Automation Conference (DAC), 2023, pp. 1–6. doi:10.1109/DAC56929.2023.10247760.
URL <https://ieeexplore.ieee.org/document/10247760>
- [10] G. Li, Y. Ding, Y. Xie, Tackling the Qubit Mapping Problem for NISQ-Era Quantum Devices, in: Proceedings of the Twenty-Fourth International Conference on Architectural Support for Programming Languages and Operating Systems, ASPLOS '19, Association for Computing Machinery, New York, NY, USA, 2019, pp. 1001–1014. doi:10.1145/3297858.3304023.
URL <https://dl.acm.org/doi/10.1145/3297858.3304023>
- [11] S. Niu, A. Suau, G. Staffelbach, A. Todri-Sanial, A Hardware-Aware Heuristic for the Qubit Mapping Problem in the NISQ Era, IEEE Transactions on Quantum Engineering 1 (2020) 1–14, arXiv:2010.03397 [quant-ph]. doi:10.1109/TQE.2020.3026544.
URL <http://arxiv.org/abs/2010.03397>
- [12] C.-Y. Huang, W.-K. Mak, Efficient Qubit Routing Using a Dynamically-Extract-and-Route Framework, IEEE Transactions on Computer-Aided Design of Integrated Circuits and Systems (2024) 1–1Conference Name: IEEE Transactions on Computer-Aided Design of Integrated Circuits and Systems. doi:10.1109/TCAD.2024.3387290.
URL <https://ieeexplore.ieee.org/document/10496462>
- [13] H. J. Manetsch, G. Nomura, E. Bataille, K. H. Leung, X. Lv, M. Endres, A tweezer array with 6100 highly coherent atomic qubits, arXiv:2403.12021

- [quant-ph] (Dec. 2024). doi:10.48550/arXiv.2403.12021.
URL <http://arxiv.org/abs/2403.12021>
- [14] Bluvstein, et al., Logical quantum processor based on reconfigurable atom arrays, *Nature* 626 (7997) (2024) 58–65, publisher: Nature Publishing Group. doi:10.1038/s41586-023-06927-3.
URL <https://www.nature.com/articles/s41586-023-06927-3>
- [15] L. Henriet, L. Beguin, A. Signoles, T. Lahaye, A. Browaeys, G.-O. Reymond, C. Jurczak, Quantum computing with neutral atoms, *Quantum* 4 (2020) 327, publisher: Verein zur Förderung des Open Access Publizierens in den Quantenwissenschaften. doi:10.22331/q-2020-09-21-327.
URL <https://quantum-journal.org/papers/q-2020-09-21-327/>
- [16] J. M. Baker, et al., Exploiting long-distance interactions and tolerating atom loss in neutral atom quantum architectures, in: *Proceedings of the 48th Annual International Symposium on Computer Architecture, ISCA '21*, IEEE Press, Virtual Event, Spain, 2021, pp. 818–831. doi:10.1109/ISCA52012.2021.00069.
URL <https://dl.acm.org/doi/10.1109/ISCA52012.2021.00069>
- [17] Y. Li, Y. Zhang, M. Chen, X. Li, P. Xu, Timing-Aware Qubit Mapping and Gate Scheduling Adapted to Neutral Atom Quantum Computing, *IEEE Transactions on Computer-Aided Design of Integrated Circuits and Systems* 42 (11) (2023) 3768–3780, conference Name: IEEE Transactions on Computer-Aided Design of Integrated Circuits and Systems. doi:10.1109/TCAD.2023.3261244.
URL <https://ieeexplore.ieee.org/document/10082942>
- [18] T. Patel, D. Silver, D. Tiwari, GRAPHINE: Enhanced Neutral Atom Quantum Computing using Application-Specific Rydberg Atom Arrangement, in: *Proceedings of the International Conference for High Performance Computing, Networking, Storage and Analysis, SC '23*, Association for Computing Machinery, New York, NY, USA, 2023, pp. 1–15. doi:10.1145/3581784.3607032.
URL <https://dl.acm.org/doi/10.1145/3581784.3607032>
- [19] B. Tan, D. Bluvstein, M. D. Lukin, J. Cong, Qubit Mapping for Reconfigurable Atom Arrays, in: *Proceedings of the 41st IEEE/ACM International Conference on Computer-Aided Design, ACM, San Diego California, 2022*, pp. 1–9. doi:10.1145/3508352.3549331.
URL <https://dl.acm.org/doi/10.1145/3508352.3549331>

- [20] B. Tan, D. Bluvstein, M. Lukin, J. Cong, Compiling Quantum Circuits for Dynamically Field-Programmable Neutral Atoms Array Processors, *Quantum* 8 (2024) 1281. doi:10.22331/q-2024-03-14-1281.
- [21] J. Ludmir, T. Patel, Parallax: A Compiler for Neutral Atom Quantum Computers under Hardware Constraints, arXiv:2409.04578 [quant-ph] (Oct. 2024). doi:10.48550/arXiv.2409.04578.
URL <http://arxiv.org/abs/2409.04578>
- [22] K. Singh, S. Anand, A. Pocklington, J. T. Kemp, H. Bernien, Dual-Element, Two-Dimensional Atom Array with Continuous-Mode Operation, *Physical Review X* 12 (1) (2022) 011040, publisher: American Physical Society. doi:10.1103/PhysRevX.12.011040.
URL <https://link.aps.org/doi/10.1103/PhysRevX.12.011040>
- [23] M. L. Bonet, J. Levy, F. Manyà, Resolution for Max-SAT, *Artificial Intelligence* 171 (8) (2007) 606–618. doi:10.1016/j.artint.2007.03.001.
URL <https://www.sciencedirect.com/science/article/pii/S0004370207000422>
- [24] E. Farhi, J. Goldstone, S. Gutmann, M. Sipser, Quantum Computation by Adiabatic Evolution, arXiv:quant-ph/0001106 (Jan. 2000). doi:10.48550/arXiv.quant-ph/0001106.
URL <http://arxiv.org/abs/quant-ph/0001106>
- [25] S. Ebadi, et al., Quantum optimization of maximum independent set using Rydberg atom arrays, *Science* 376 (6598) (2022) 1209–1215, publisher: American Association for the Advancement of Science. doi:10.1126/science.abo6587.
URL <https://www.science.org/doi/full/10.1126/science.abo6587>

Appendix A. Quantum Circuit Basics

Quantum computing is a computational paradigm that leverages quantum properties to perform calculations. It is typically implemented using quantum circuits, where the fundamental unit of computation is the qubit. By applying quantum gates to create entanglement and execute carefully designed operations, quantum circuits have the potential to solve a wide range of problems.

Fig. A.10 illustrates a quantum circuit consisting of 4 qubits and 8 gates, where gates $g_0 \sim g_3$ are single qubit gates and gates $g_4 \sim g_7$ are two-qubit gates employed to establish entanglement between qubits. By performing measurement operations, we can obtain the output of a quantum circuit.

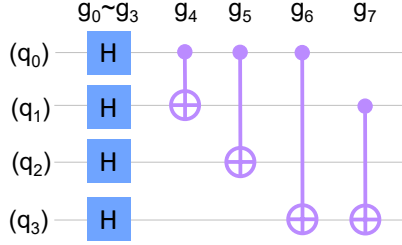


Figure A.10: Demonstration of a quantum circuit.

Similar to programs running on classical computers, quantum circuits must be deployed on quantum computers for execution. The compilation of quantum circuits involves transforming a quantum circuit into an executable sequence of operations that can be implemented on quantum hardware to achieve the intended functionality. The quantum compilation approach varies significantly depending on the underlying quantum hardware architecture, and this basic understanding of quantum circuits provides the foundation for appreciating the unique compilation challenges.

Appendix B. Detailed Experimental Setup

Metrics for evaluating compilation performance focused on both efficiency and quality. Compilation efficiency was assessed through solution time and speedup ratio measurements. Solution time records the total time required to complete the quantum circuit compilation process. A computation time limit of 10,000 seconds was imposed on all compilation methods. If the compilation process exceeded this threshold, it was considered a timeout, and no valid solution was recorded. The speedup ratio was calculated as the ratio of solution times between DPQA and PAC, indicating how many times faster PAC completed the compilation compared

to the baseline method. Compilation quality was evaluated using the number of quantum circuit layers produced after compilation. A smaller number of layers generally indicates higher quality compilation as it leads to shorter execution times on quantum hardware. The layer reduction ratio was calculated using Equation 6.

Benchmarks used in the evaluation consisted of 40 random 3-regular graph circuits with qubit counts ranging from 60 to 90 and two-qubit gate counts from 90 to 135. These circuits were generated using a standard procedure for creating random regular graphs, where each vertex (qubit) has exactly three connections to other vertices. The circuits are structurally identical to those used in DPQA evaluation to ensure fair comparison. These 3-regular graph circuits were selected because they represent a wide range of quantum algorithms for combinatorial optimization problems. They are particularly relevant for applications such as Max-Cut optimization and multiple problem scenarios including Quantum Adiabatic Optimization Algorithm (QAOA) and trotterized adiabatic evolution. The structure of these circuits provides a realistic test case for evaluating compilation performance in practical quantum computing scenarios.

Hardware configurations for the neutral atom quantum computer included multiple array dimensions to comprehensively evaluate scalability. The configurations ranged from 16×16 arrays representing current proposed systems, through intermediate sizes of 20×20 , 24×24 , and 28×28 , to large-scale configurations of 50×50 and 64×64 representing long-term scalability targets. These configurations were selected to evaluate performance across a spectrum of system sizes, from currently feasible implementations to potential future large-scale systems. This range allows for the assessment of how compilation performance scales with increasing system size, which is a critical factor for practical quantum computing applications.

Environment for all experiments utilized consistent hardware and software configurations to ensure fair comparison. Experiments were conducted on a Ryzen 9 7900X CPU running at 4.7GHz with 32GB of RAM, providing sufficient computational resources for evaluating compilation performance across various circuit and system sizes. The software environment consisted of Linux operating system, Python 3.9, Qiskit 1.0.0 for quantum circuit representation, NetworkX 3.2.1 for graph manipulation and analysis, and Z3 4.12.5.0 as the SMT solver for constraint satisfaction. The implementation of PAC utilized the same core solver mechanisms as DPQA, with the primary differences being the hardware plane partitioning and quantum circuit division components described in the main text.

Appendix C. Experimentation on series array size

Table C.4 presents the results for a 20×20 array. PAC completed all circuit compilations within 1000 seconds. The highest speedup was $96.56\times$ on the benchmark `rand3reg_70_0`, and the average speedup across circuits compilable by DPQA reached $60.86\times$. Regarding circuit depth, PAC outperformed DPQA with an average reduction of 0.43 layers.

As shown in Table C.5, PAC completed all compilations in under 300 seconds on the 24×24 array. The maximum speedup reached $202.81\times$ on `rand3reg_70_1`, and the average speedup on DPQA-solvable circuits was $102.56\times$, implying PAC required less than 1% of DPQA’s time on average. In terms of quality, PAC maintained comparable circuit depth, with DPQA and PAC averaging 12.48 and 12.67 layers, respectively.

Table C.6 reports results for a 28×28 array. PAC achieved up to $112.84\times$ speedup on `rand3reg_80_3` and completed all circuits within 300 seconds. The average acceleration over DPQA was $56.54\times$. PAC’s average compiled circuit depth was 13.14, close to DPQA’s 12.76, demonstrating comparable quality across most circuits.

Table C.7 shows the results for a 50×50 array. PAC achieved a maximum speedup of $98.96\times$ on `rand3reg_80_5`, with all compilation times remaining below 300 seconds. On circuits solvable by DPQA, the average speedup was $61.4\times$. The average circuit depths were 12.96 for PAC and 12.77 for DPQA, indicating PAC’s significant efficiency gains without compromising output quality.

These results from intermediate array sizes consistently support the trend observed in the main text: PAC demonstrates substantial performance advantages across all tested architectures while maintaining compilation quality comparable to DPQA. The speedup factors range from approximately $50\times$ to over $200\times$ depending on the specific circuit and array configuration, with compilation times consistently remaining under 1200 seconds even for the most complex circuits. This performance characteristic is particularly valuable for neutral atom quantum computing, where larger architectures are expected to become available as the technology matures.

Table C.4: Solving Time and Circuit Layers on 20×20 Array.

Quantum Circuit	Qubits	Solving time (s)			Circuit Layers			
		DPQA	PAC	Speedup	DPQA	PAC	Δ_{cl}	R_{cl}
rand3reg_60_0	60	1778.16	42.92	41.43 ↑	13	13	0	0.00%
rand3reg_60_1	60	1891.21	32.43	58.31 ↑	12	12	0	0.00%
rand3reg_60_2	60	2213.82	32.89	67.31 ↑	13	12	-1	-7.69%
rand3reg_60_3	60	1659.24	35.22	47.12 ↑	12	12	0	0.00%
rand3reg_60_4	60	1731.69	36.90	46.94 ↑	13	11	-2	-15.38%
rand3reg_60_5	60	1332.27	36.21	36.79 ↑	11	11	0	0.00%
rand3reg_60_6	60	2016.17	31.10	64.83 ↑	12	11	-1	-8.33%
rand3reg_60_7	60	1628.87	39.38	41.37 ↑	15	12	-3	-20.00%
rand3reg_60_8	60	2183.50	36.22	60.29 ↑	12	12	0	0.00%
rand3reg_60_9	60	1442.68	37.77	38.19 ↑	11	12	1	9.09%
rand3reg_70_0	70	6438.56	66.68	96.56 ↑	14	14	0	0.00%
rand3reg_70_1	70	5241.48	68.91	76.07 ↑	14	14	0	0.00%
rand3reg_70_2	70	5418.36	82.97	65.31 ↑	14	13	-1	-7.14%
rand3reg_70_3	70	4024.76	84.12	47.85 ↑	13	13	0	0.00%
rand3reg_70_4	70	5930.30	92.84	63.88 ↑	13	13	0	0.00%
rand3reg_70_5	70	3882.56	79.52	48.82 ↑	13	12	-1	-7.69%
rand3reg_70_6	70	5378.81	64.77	83.05 ↑	13	14	1	7.69%
rand3reg_70_7	70	4280.42	64.02	66.86 ↑	15	13	-2	-13.33%
rand3reg_70_8	70	4359.31	59.55	73.21 ↑	13	12	-1	-7.69%
rand3reg_70_9	70	4952.12	69.23	71.53 ↑	13	13	0	0.00%
rand3reg_80_0	80	9166.24	111.32	82.34 ↑	14	15	1	7.14%
rand3reg_80_1	80	TO	125.70	>79.56 ↑	-	15	-	-
rand3reg_80_2	80	TO	143.36	>69.76 ↑	-	15	-	-
rand3reg_80_3	80	TO	144.07	>69.41 ↑	-	16	-	-
rand3reg_80_4	80	TO	946.88	>10.56 ↑	-	15	-	-
rand3reg_80_5	80	TO	139.32	>71.78 ↑	-	15	-	-
rand3reg_80_6	80	TO	132.34	>75.56 ↑	-	13	-	-
rand3reg_80_7	80	TO	148.79	>67.21 ↑	-	16	-	-
rand3reg_80_8	80	TO	129.66	>77.13 ↑	-	15	-	-
rand3reg_80_9	80	TO	217.81	>45.91 ↑	-	13	-	-
rand3reg_90_0	90	TO	369.19	>27.09 ↑	-	15	-	-
rand3reg_90_1	90	TO	243.11	>41.13 ↑	-	17	-	-
rand3reg_90_2	90	TO	493.55	>20.26 ↑	-	16	-	-
rand3reg_90_3	90	TO	857.46	>11.66 ↑	-	15	-	-
rand3reg_90_4	90	TO	246.16	>40.62 ↑	-	16	-	-
rand3reg_90_5	90	TO	221.91	>45.06 ↑	-	16	-	-
rand3reg_90_6	90	TO	309.86	>32.27 ↑	-	15	-	-
rand3reg_90_7	90	TO	302.84	>33.02 ↑	-	16	-	-
rand3reg_90_8	90	TO	509.51	>19.63 ↑	-	16	-	-
rand3reg_90_9	90	TO	228.26	>43.81 ↑	-	16	-	-
		3664.31	57.38	60.86 ↑	13	12.57	-0.43	-3.30%

Table C.5: Solving Time and Circuit Layers on 24×24 Array.

Quantum Circuit	Qubits	Solving time (s)			Circuit Layers			
		DPQA	PAC	Speedup	DPQA	PAC	Δ_{cl}	R_{cl}
rand3reg_60_0	60	1550.36	21.52	72.03 ↑	11	12	1	9.09%
rand3reg_60_1	60	1774.67	168.35	10.54 ↑	11	12	1	9.09%
rand3reg_60_2	60	1618.20	25.06	64.56 ↑	12	12	0	0.00%
rand3reg_60_3	60	2196.41	33.01	66.54 ↑	12	13	1	8.33%
rand3reg_60_4	60	1985.55	25.57	77.64 ↑	13	13	0	0.00%
rand3reg_60_5	60	2191.97	22.86	95.91 ↑	12	12	0	0.00%
rand3reg_60_6	60	2038.84	20.37	100.11 ↑	12	11	-1	-8.33%
rand3reg_60_7	60	1881.91	22.05	85.36 ↑	12	12	0	0.00%
rand3reg_60_8	60	1367.69	22.66	60.37 ↑	11	12	1	9.09%
rand3reg_60_9	60	1433.10	26.96	53.15 ↑	13	13	0	0.00%
rand3reg_70_0	70	7590.54	42.97	176.66 ↑	12	13	1	8.33%
rand3reg_70_1	70	6811.90	33.59	202.81 ↑	13	13	0	0.00%
rand3reg_70_2	70	5301.34	49.09	107.98 ↑	12	13	1	8.33%
rand3reg_70_3	70	4852.27	39.96	121.43 ↑	13	13	0	0.00%
rand3reg_70_4	70	4262.68	46.16	92.35 ↑	12	13	1	8.33%
rand3reg_70_5	70	5838.08	35.38	165.01 ↑	13	13	0	0.00%
rand3reg_70_6	70	6825.88	50.74	134.53 ↑	15	14	-1	-6.67%
rand3reg_70_7	70	6614.11	38.10	173.62 ↑	12	13	1	8.33%
rand3reg_70_8	70	5175.00	120.03	43.11 ↑	14	14	0	0.00%
rand3reg_70_9	70	4716.40	38.33	123.05 ↑	13	12	-1	-7.69%
rand3reg_80_0	80	TO	80.61	>124.06 ↑	-	14	-	-
rand3reg_80_1	80	TO	78.76	>126.97 ↑	-	14	-	-
rand3reg_80_2	80	8185.80	64.42	127.08 ↑	14	13	-1	-7.14%
rand3reg_80_3	80	TO	78.24	>127.81 ↑	-	13	-	-
rand3reg_80_4	80	TO	92.88	>107.66 ↑	-	14	-	-
rand3reg_80_5	80	TO	103.84	>96.30 ↑	-	13	-	-
rand3reg_80_6	80	TO	81.09	>123.32 ↑	-	15	-	-
rand3reg_80_7	80	TO	75.62	>132.25 ↑	-	14	-	-
rand3reg_80_8	80	TO	84.87	>117.83 ↑	-	14	-	-
rand3reg_80_9	80	TO	78.45	>127.47 ↑	-	14	-	-
rand3reg_90_0	90	TO	146.52	>68.25 ↑	-	17	-	-
rand3reg_90_1	90	TO	143.11	>69.88 ↑	-	18	-	-
rand3reg_90_2	90	TO	149.88	>66.72 ↑	-	17	-	-
rand3reg_90_3	90	TO	178.82	>55.92 ↑	-	16	-	-
rand3reg_90_4	90	TO	145.14	>68.90 ↑	-	17	-	-
rand3reg_90_5	90	TO	214.41	>46.64 ↑	-	17	-	-
rand3reg_90_6	90	TO	134.41	>74.40 ↑	-	16	-	-
rand3reg_90_7	90	TO	163.04	>61.33 ↑	-	16	-	-
rand3reg_90_8	90	TO	181.15	>55.20 ↑	-	17	-	-
rand3reg_90_9	90	TO	137.61	>72.67 ↑	-	16	-	-
		4010.13	82.39	96.94 ↑	12.47619	13.95	0.190476	1.53%

Table C.6: Solving Time and Circuit Layers on 28×28 Array.

Quantum Circuit	Qubits	Solving time (s)			Circuit Layers			
		DPQA	PAC	Speedup	DPQA	PAC	Δ_{cl}	R_{cl}
rand3reg_60_0	60	786.15	33.84	23.23 ↑	10	11	1	10.00%
rand3reg_60_1	60	1432.49	30.10	47.60 ↑	11	12	1	9.09%
rand3reg_60_2	60	1430.77	80.86	17.69 ↑	14	14	0	0.00%
rand3reg_60_3	60	1050.69	31.74	33.11 ↑	12	12	0	0.00%
rand3reg_60_4	60	1365.81	33.16	41.19 ↑	11	12	1	9.09%
rand3reg_60_5	60	1204.43	32.27	37.32 ↑	11	12	1	9.09%
rand3reg_60_6	60	1016.73	29.97	33.93 ↑	12	12	0	0.00%
rand3reg_60_7	60	1508.19	26.76	56.36 ↑	12	12	0	0.00%
rand3reg_60_8	60	1089.72	26.02	41.88 ↑	12	11	-1	-8.33%
rand3reg_60_9	60	1292.18	37.48	34.48 ↑	12	13	1	8.33%
rand3reg_70_0	70	3367.48	47.75	70.52 ↑	13	14	1	7.69%
rand3reg_70_1	70	3548.97	68.26	51.99 ↑	14	13	-1	-7.14%
rand3reg_70_2	70	2672.21	56.76	47.08 ↑	12	13	1	8.33%
rand3reg_70_3	70	2716.01	59.95	45.31 ↑	12	13	1	8.33%
rand3reg_70_4	70	3246.66	60.65	53.53 ↑	13	13	0	0.00%
rand3reg_70_5	70	2995.02	77.49	38.65 ↑	13	14	1	7.69%
rand3reg_70_6	70	3165.55	52.51	60.28 ↑	14	14	0	0.00%
rand3reg_70_7	70	2893.17	41.00	70.56 ↑	13	13	0	0.00%
rand3reg_70_8	70	3170.81	47.11	67.30 ↑	13	13	0	0.00%
rand3reg_70_9	70	2793.77	39.55	70.64 ↑	12	12	0	0.00%
rand3reg_80_0	80	7376.53	110.48	66.77 ↑	13	14	1	7.69%
rand3reg_80_1	80	8453.08	89.04	94.94 ↑	13	14	1	7.69%
rand3reg_80_2	80	8623.65	84.29	102.31 ↑	13	13	0	0.00%
rand3reg_80_3	80	TO	88.62	>112.84 ↑	-	14	-	-
rand3reg_80_4	80	6353.21	105.38	60.29 ↑	14	14	0	0.00%
rand3reg_80_5	80	7241.10	97.74	74.08 ↑	15	15	0	0.00%
rand3reg_80_6	80	7570.55	100.30	75.48 ↑	14	14	0	0.00%
rand3reg_80_7	80	9909.30	101.30	97.82 ↑	15	15	0	0.00%
rand3reg_80_8	80	7148.20	105.37	67.84 ↑	14	15	1	7.14%
rand3reg_80_9	80	5914.57	103.10	57.37 ↑	13	14	1	7.69%
rand3reg_90_0	90	TO	168.48	>59.35 ↑	-	15	-	-
rand3reg_90_1	90	TO	175.44	>57.00 ↑	-	16	-	-
rand3reg_90_2	90	TO	187.09	>53.45 ↑	-	16	-	-
rand3reg_90_3	90	TO	146.01	>68.49 ↑	-	16	-	-
rand3reg_90_4	90	TO	128.03	>78.11 ↑	-	15	-	-
rand3reg_90_5	90	TO	294.32	>33.98 ↑	-	16	-	-
rand3reg_90_6	90	TO	181.32	>55.15 ↑	-	16	-	-
rand3reg_90_7	90	TO	168.31	>59.41 ↑	-	16	-	-
rand3reg_90_8	90	TO	233.97	>42.74 ↑	-	17	-	-
rand3reg_90_9	90	TO	237.35	>42.13 ↑	-	17	-	-
		3839.21	62.42	56.54 ↑	12.75862	13.13793	0.37931	2.97%

Table C.7: Solving Time and Circuit Layers on 50×50 Array.

Quantum Circuit	Qubits	Solving time (s)			Circuit Layers			
		DPQA	PAC	Speedup	DPQA	PAC	Δ_{cl}	R_{cl}
rand3reg_60_0	60	1641.12	20.87	78.64 ↑	13	11	-2	-15.38%
rand3reg_60_1	60	1336.53	28.83	46.37 ↑	12	13	1	8.33%
rand3reg_60_2	60	1190.10	29.62	40.18 ↑	11	12	1	9.09%
rand3reg_60_3	60	1951.21	34.64	56.32 ↑	13	13	0	0.00%
rand3reg_60_4	60	1352.02	28.02	48.25 ↑	13	13	0	0.00%
rand3reg_60_5	60	1481.97	31.44	47.13 ↑	12	12	0	0.00%
rand3reg_60_6	60	1139.93	21.96	51.91 ↑	10	11	1	10.00%
rand3reg_60_7	60	1425.03	23.44	60.79 ↑	11	11	0	0.00%
rand3reg_60_8	60	1404.06	28.13	49.92 ↑	12	12	0	0.00%
rand3reg_60_9	60	1173.01	30.52	38.43 ↑	12	13	1	8.33%
rand3reg_70_0	70	3913.59	65.65	59.61 ↑	14	14	0	0.00%
rand3reg_70_1	70	3314.47	49.84	66.50 ↑	13	12	-1	-7.69%
rand3reg_70_2	70	3127.76	52.40	59.69 ↑	12	13	1	8.33%
rand3reg_70_3	70	2982.15	49.65	60.06 ↑	13	13	0	0.00%
rand3reg_70_4	70	2329.54	39.94	58.32 ↑	11	12	1	9.09%
rand3reg_70_5	70	2566.87	53.01	48.42 ↑	12	13	1	8.33%
rand3reg_70_6	70	2702.81	47.09	57.40 ↑	12	13	1	8.33%
rand3reg_70_7	70	4330.19	46.45	93.21 ↑	14	12	-2	-14.29%
rand3reg_70_8	70	3272.70	47.07	69.53 ↑	13	14	1	7.69%
rand3reg_70_9	70	3927.84	43.08	91.18 ↑	13	13	0	0.00%
rand3reg_80_0	80	TO	138.86	>72.02 ↑	-	14	-	-
rand3reg_80_1	80	7892.75	88.17	89.52 ↑	15	14	-1	-6.67%
rand3reg_80_2	80	7453.59	86.94	85.74 ↑	13	14	1	7.69%
rand3reg_80_3	80	7102.36	153.01	46.42 ↑	15	15	0	0.00%
rand3reg_80_4	80	8591.70	117.77	72.95 ↑	13	14	1	7.69%
rand3reg_80_5	80	TO	101.05	>98.96 ↑	-	14	-	-
rand3reg_80_6	80	7234.03	114.87	62.98 ↑	15	15	0	0.00%
rand3reg_80_7	80	TO	104.75	>95.47 ↑	-	15	-	-
rand3reg_80_8	80	TO	110.31	>90.65 ↑	-	15	-	-
rand3reg_80_9	80	6831.75	119.99	56.93 ↑	15	15	0	0.00%
rand3reg_90_0	90	TO	209.22	>47.80 ↑	-	16	-	-
rand3reg_90_1	90	TO	215.17	>46.48 ↑	-	16	-	-
rand3reg_90_2	90	TO	158.44	>63.12 ↑	-	16	-	-
rand3reg_90_3	90	TO	160.93	>62.14 ↑	-	14	-	-
rand3reg_90_4	90	TO	176.66	>56.60 ↑	-	16	-	-
rand3reg_90_5	90	TO	188.09	>53.17 ↑	-	16	-	-
rand3reg_90_6	90	TO	233.19	>42.88 ↑	-	16	-	-
rand3reg_90_7	90	TO	161.04	>62.10 ↑	-	15	-	-
rand3reg_90_8	90	TO	183.16	>54.60 ↑	-	16	-	-
rand3reg_90_9	90	TO	147.69	>67.71 ↑	-	16	-	-
		3525.73	55.86	61.40 ↑	12.76923	12.96154	0.192308	1.51%